energies

Article

Performance Analysis of Energy-Harvesting Amplify-and-Forward Relaying with Fluid Antenna Systems

Khalid Yahya [1,2,*], Mahmoud Aldababsa [3,*], Banafsheh Alizadeh Arashloo [4], Saleh Al Dawsari [5,6,*] and Sajjad Ahmad Khan [7]

1 Institute of Research and Development, Duy Tan University, Da Nang 550000, Vietnam
2 School of Engineering & Technology, Duy Tan University, Da Nang 550000, Vietnam
3 Department of Electrical and Electronics Engineering, Nisantasi University, Istanbul 34398, Türkiye
4 Department of Electrical and Electronics Engineering, Faculty of Engineering and Architecture, Istanbul Gelisim University, Istanbul 34310, Türkiye; balizadeh@gelisim.edu.tr
5 School of Engineering, Cardiff University, Cardiff CF24 3AA, UK
6 Electrical Engineering Department, College of Engineering, Najran University, Najran P.O. Box 1988, Saudi Arabia
7 Department of Software Engineering, Faculty of Engineering, Kocaeli University, Izmit 41001, Türkiye; sajjadahmad.khan@kocaeli.edu.tr
* Correspondence: halityahya@duytan.edu.tr (K.Y.); mahmoud.aldababsa@nisantasi.edu.tr (M.A.); aldawsarisa@cardiff.ac.uk (S.A.D.)

Abstract

This paper studies a cooperative wireless system in which a single-antenna base station (BS) communicates with a destination user (U) via a half-duplex energy-harvesting amplify-and-forward relay, while the direct BS–U link is unavailable. The destination (U) is equipped with a fluid antenna system (FAS) comprising multiple closely spaced receive ports, enabling spatial reconfigurability through instantaneous port selection. A power-splitting architecture is adopted at the relay to support simultaneous energy harvesting and information forwarding. All wireless links are modeled as flat Rayleigh fading, and the spatial correlation among the FAS ports is explicitly incorporated. To analytically characterize the impact of correlated port selection, a Gaussian copula framework is employed to model the joint distribution of the FAS-channel power gains. Exact integral expressions for the cumulative distribution function of the end-to-end signal-to-noise ratio are derived, from which the outage probability is obtained. For the special case of uncorrelated FAS ports, closed-form expressions are further developed using order statistics and special functions. In addition, asymptotic analysis is carried out to provide further insight into system performance in the high-signal-to-noise-ratio region. Numerical and Monte Carlo simulation results validate the analytical derivations and demonstrate that FAS-based receiver selection yields significant gains in outage performance, even in the presence of strong spatial correlation and energy-harvesting constraints.

Keywords: fluid antenna system; energy harvesting; amplify-and-forward relaying; cooperative communications; outage probability; Gaussian copula; spatial correlation

Academic Editors: Pratik Goswami and Adeel Iqbal

Received: 24 May 2026
Revised: 22 July 2026
Accepted: 23 July 2026
Published: 25 July 2026

1. Introduction

Beyond-fifth-generation (B5G) and sixth-generation (6G) wireless networks are expected to support dense, reliable, and energy-efficient connectivity in environments where blockage, shadowing, and device-energy limitations become increasingly severe [1–5]. These requirements naturally motivate cooperative relaying and energy harvesting (EH).

Relaying helps preserve connectivity when the direct base-station (BS)–user (U) path is unavailable, while EH can reduce the dependence of relay nodes on fixed power supplies and frequent battery replacement [6–9]. Still, EH amplify-and-forward (AF) relaying is not a simple extension of conventional relaying. Its reliability depends jointly on the two-hop fading process, the harvested relay power, and the noise amplified by the relay.

Fluid antenna systems (FASs) provide another useful degree of freedom. By allowing a receiver to select the most favorable port among several candidate positions inside a compact region, FAS can exploit spatial channel variations without requiring many widely separated antennas or multiple radio-frequency chains [10,11]. This is attractive for compact and energy-constrained wireless devices. However, the gain is not ideal in practice. Since FAS ports are usually closely spaced, their channel gains can be spatially correlated; therefore, assuming independent ports may overestimate the diversity benefit obtained from port selection [12].

Several recent studies have investigated FAS, fluid-antenna relay (FAR), and EH-assisted relaying from different viewpoints. Some papers focus on antenna location or resource optimization. Others consider FAR-assisted reliability, finite-block-length FAS transmission, or EH-AF relaying without destination-side FAS correlation. To make the novelty clearer, Table 1 summarizes the closest studies and highlights how the proposed scheme differs from them.

Table 1. Comparison with recent FAS, FAR, and EH-assisted relay studies.

Reference	Main Focus	FAS/FAR/EH-Relay Aspect	Key Difference
New et al. [10]; Shah et al. [11]	General FAS/FAMA concepts for 6G systems	FAS principles, diversity, and compact spatial reconfigurability	No EH-AF outage model.
Ramírez-Espinosa et al. [12]	Spatial block-correlation modeling for FAS channels	Correlation-aware FAS channel modeling	No relay or EH link.
Xu et al. [13]	FAR-assisted communication with antenna-location optimization	FAR placement and antenna-location design	Optimization, not EH-AF outage.
Aka et al. [14]	Power minimization for half-duplex FAS-enabled relaying	FAS-enabled relay with power optimization	No power-splitting EH analysis.
Xu et al. [15]	Energy-efficient FAR-assisted wireless communication	FAR placement, fluid-antenna positions, power control, and beamforming	Energy efficiency, not outage.
Xu et al. [16]	Fair-rate maximization in FAR-assisted multi-user MISO systems	FAR-assisted multi-user rate optimization	No EH–AF reliability model.
Xu et al. [17]	Energy-efficient FAR-assisted wireless networks	Network-level FAR energy-efficiency optimization	No correlated FAS receiver selection.
Xu et al. [18]	FAR-assisted communication with hybrid relaying-scheme selection	Hybrid AF/DF FAR relaying and outage-oriented design	No power-splitting EH relay.
Xu et al. [19]	Performance of FAR-assisted AAV–NOMA networks	FAR-assisted AF/DF relaying with Gaussian copula-based analysis	Different AAV–NOMA system.
Xin et al. [20]	Energy-efficiency resource allocation for EH–AF relaying	RF–EH–AF relaying with resource allocation	No FAS port correlation.
Singh and Garg [21]	Performance analysis of two-way AF relaying with EH	EH-assisted AF relay performance	No FAS/FAR ports.
Kapucu and Bilim [22]	ASER analysis of FAS with rectangular and hexagonal QAM	FAS physical-layer error-rate analysis	No relay or EH model.
Zhang et al. [23]	Finite-block-length FAS transmission with spatial block correlation	Short-packet FAS reliability under correlated ports	No EH–AF relaying.
Proposed scheme	**Outage analysis of a blockage-limited EH–AF relay-assisted FAS system**	**Power-splitting EH–AF relay, blocked direct BS–U link, and correlated destination-side FAS receive-port selection**	

As shown in Table 1, the existing literature provides important foundations for FAS operation, FAS correlation modeling, FAR-assisted optimization, EH–AF resource allocation, and FAR-based reliability analysis. These studies are highly relevant. However, the specific reliability problem considered here has not been fully characterized: a blockage-limited cooperative link where the BS communicates with the destination only through a power-splitting EH–AF relay, while the destination applies FAS receiver-port selection under spatially correlated fading. This gap is important because EH constraints and AF noise amplification already limit the end-to-end SNR, and the correlation among FAS ports can further reduce the practical diversity gain.

Motivated by this gap, the proposed scheme develops a correlation-aware outage analysis for an EH–AF relay-assisted FAS system. The destination is equipped with an N-port FAS and selects the port with the maximum instantaneous relay–user channel gain. Unlike independent-port models, the dependence among the closely spaced FAS ports is captured through a Gaussian copula with Rayleigh fading marginals. In this way, the analysis keeps the marginal fading model tractable while still accounting for the statistical dependence that appears in compact FAS implementations.

Contributions

The main contributions of this paper are summarized as follows:

- We formulate a blockage-limited cooperative communication system in which a single-antenna BS communicates with a destination (U) only through a half-duplex EH–AF relay. The destination employs an N-port FAS and selects the receive port with the maximum instantaneous relay–user channel gain.
- We develop a correlation-aware analytical model for FAS-based receive-port selection. The dependence among the closely spaced FAS ports is represented using a Gaussian copula with Rayleigh fading marginals, which provides a more realistic alternative to the independent-port assumption.
- We derive exact integral-form expressions for the cumulative distribution function of the end-to-end signal-to-noise ratio and the corresponding outage probability under correlated FAS ports. These expressions capture the joint impact of EH, AF relaying, and spatially correlated receive-port selection.
- For the uncorrelated-port benchmark, we obtain closed-form outage expressions using order statistics and special-function representations. We further derive asymptotic expressions to characterize the high-SNR behavior and provide additional insight into the achievable diversity performance. This benchmark provides a clear reference for quantifying the performance loss caused by FAS port correlation.
- We validate the analytical results through Monte Carlo simulations and provide design insights into the effects of the number of FAS ports, spatial correlation, energy-conversion efficiency, the power-splitting ratio, and the average transmit SNR on system reliability.

The remainder of this paper is organized as follows. Section 2 presents the EH–AF relay-assisted FAS system model. Section 3 develops the end-to-end SNR statistics using the Gaussian copula-based selected-port distribution. Section 4 derives the outage probability for correlated and uncorrelated FAS ports. Section 5 concludes the paper.

2. System Model

In this paper, we consider a cooperative wireless communication system in which a single-antenna BS communicates with a destination (U) via a single-antenna (R). R operates as half-duplex EH–AF node. At the same time, U is equipped with a FAS comprising N candidate receive ports, enabling dynamic port selection to exploit spatial channel variations. The direct BS–U link is assumed to be blocked due to severe path loss and shadowing effects caused by obstacles such as buildings, terrain irregularities, or dense urban structures, which makes reliable direct transmission infeasible. Consequently, all information exchange between the BS and the U is realized exclusively through the R node.

The considered cooperative communication architecture is illustrated in Figure 1, where the blocked direct BS–U link, the EH–AF relay with power splitting, and the FAS-enabled destination user are explicitly shown.

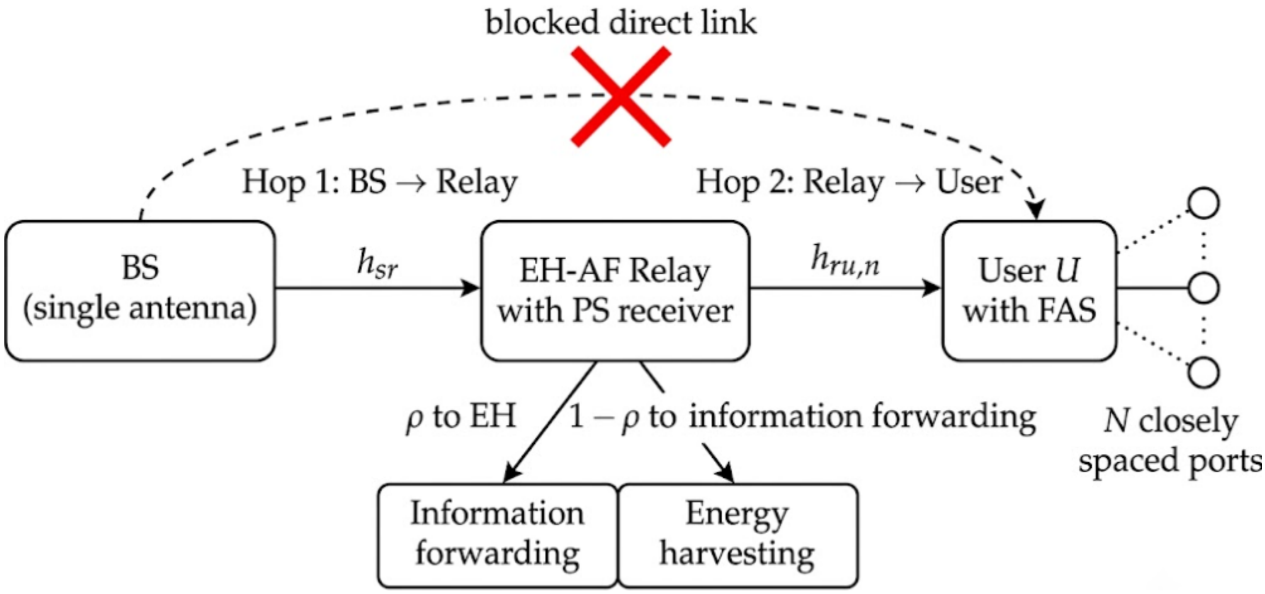

Figure 1. System model of the EH–AF relay-assisted FAS communication system.

As shown in Figure 1, the transmission is performed over two hops: the BS first sends the information signal to the EH–AF relay; the relay then forwards the amplified signal to the destination user, where FAS-based receive-port selection is applied.

All wireless links experience flat Rayleigh fading. Let h_{sr} denote the BS–R channel coefficient. The R–U channel coefficients over the N FAS ports are collected in the vector expressed as $\mathbf{h}_{ru} = \left[h_{ru,1}, \ldots, h_{ru,n}, \ldots, h_{ru,N}\right]^{\mathrm{T}}$, where $h_{ru,n}$ denotes the channel coefficient between R and the n-th FAS port of U. The channels are modeled as $h_{sr} \sim \mathcal{CN}(0, \Omega_{sr})$ and $\mathbf{h}_{ru} \sim \mathcal{CN}\big(\mathbf{0}, \Omega_{ru}\mathbf{R}\big)$, where Ω_{sr} and Ω_{ru} are the average channel powers of the BS–R and R–U links, respectively. Additionally, $\mathbf{R} \in \mathbb{C}^{N\times N}$ is the FAS spatial correlation matrix. The (i, j)-th entry of $\mathbf{R}$ is $[\mathbf{R}]_{i,j} = \frac{\mathbb{E}\left\{h_{ru,i}h^*_{ru,j}\right\}}{\Omega_{ru}}$, which captures the statistical dependence across the closely spaced fluid ports. Under Jakes' isotropic scattering assumption, a commonly adopted model is [24]

$$[\mathbf{R}]_{i,j} = J_0\left(2\pi\frac{d_{i,j}}{\lambda}\right), \tag{1}$$

where $d_{i,j}$ denotes the distance between ports i and j and λ is the carrier wavelength. The additive noises at R and U are independent circularly symmetric, complex Gaussian random variables, i.e., $w_r \sim \mathcal{CN}(0, \sigma_r^2)$ and $w_u \sim \mathcal{CN}(0, \sigma_u^2)$. The transmission occurs over two orthogonal phases (time slots). In the first phase, BS-to-R transmission, the BS transmits a unit-power symbol (x) with $\mathbb{E}\{|x|^2\} = 1$ and transmit power (P_s). The received signal at R is

$$y_r = \sqrt{P_s}\,h_{sr}x + w_r. \tag{2}$$

R employs a power-splitting (PS) architecture for simultaneous information relaying and EH. Specifically, a fraction ($\rho \in (0, 1)$) of the received signal power is allocated to the EH circuit, while the remaining fraction $(1-\rho)$ is used for information processing [25]. Accordingly, the information-processing (IP) branch signal is

$$y_r^{(\mathrm{IP})} = \sqrt{1-\rho}\,y_r, \tag{3}$$

and the harvested transmit power at R is modeled as

$$P_r = \eta \rho P_s |h_{sr}|^2, \tag{4}$$

where $\eta \in (0,1]$ denotes the energy conversion efficiency.

In the second phase, R forwards an amplified version of the IP-branch signal:

$$x_r = G\, y_r^{(\mathrm{IP})} = G\sqrt{1-\rho}\, y_r, \tag{5}$$

where G is the AF amplification gain. Enforcing the instantaneous R transmit power constraint yields the exact variable-gain form [26]:

$$G = \sqrt{\frac{P_r}{(1-\rho)\left(P_s|h_{sr}|^2 + \sigma_r^2\right)}} = \sqrt{\frac{\eta\rho P_s|h_{sr}|^2}{(1-\rho)\left(P_s|h_{sr}|^2 + \sigma_r^2\right)}}. \tag{6}$$

Following the standard approximation adopted in the EH–AF literature (neglecting σ_r^2 in the denominator when $\sigma_r^2 \ll P_s|h_{sr}|^2$), the gain simplifies to [27]

$$G \approx \sqrt{\frac{\eta\rho}{1-\rho}}. \tag{7}$$

Note that the received-signal, SNR, CDF, and OP expressions derived in the sequel are exact for the adopted high-SNR approximated gain model, which has been widely used in related EH–AF relay studies and preserves the dominant system behavior in the moderate-to-high SNR regime.

The received signal at the n-th FAS port of U is

$$\begin{aligned} y_{u,n} &= h_{ru,n} x_r + w_u \\ &= h_{ru,n}\, G\sqrt{1-\rho}\left(\sqrt{P_s}\, h_{sr} x + w_r\right) + w_u \\ &= G\sqrt{(1-\rho)P_s}\, h_{sr} h_{ru,n} x + G\sqrt{1-\rho}\, h_{ru,n} w_r + w_u. \end{aligned} \tag{8}$$

Using (7), we further obtain the convenient equivalent form:

$$y_{u,n} \approx \underbrace{\sqrt{\eta\rho P_s}\, h_{sr} h_{ru,n} x}_{\text{desired signal}} + \underbrace{\sqrt{\eta\rho}\, h_{ru,n} w_r + w_u}_{\text{noise}}. \tag{9}$$

The instantaneous end-to-end SNR at the n-th port ($\gamma_{e2e,n}$) is defined as the ratio between the instantaneous desired-signal power and the total noise power, i.e., $\gamma_{e2e,n} \triangleq \frac{\mathbb{E}\{|\text{desired signal}|^2\}}{\mathbb{E}\{|\text{noise}|^2\}}$, where the expectations are taken with respect to the data symbol and noise terms, conditioned on the channel realizations. Since $\mathbb{E}\{|x|^2\} = 1$, $w_r \sim \mathcal{CN}(0, \sigma_r^2)$, and $w_u \sim \mathcal{CN}(0, \sigma_u^2)$, the power of each term in (9) is obtained as follows:

$$\mathbb{E}\left\{|\text{desired signal}|^2\right\} = \mathbb{E}\left\{\left|\sqrt{\eta\rho P_s}\, h_{sr} h_{ru,n} x\right|^2\right\} = \eta\rho P_s |h_{sr}|^2 |h_{ru,n}|^2, \tag{10}$$

$$\mathbb{E}\left\{|\text{noise}|^2\right\} = \mathbb{E}\left\{|\sqrt{\eta\rho}\, h_{ru,n} w_r|^2 + |w_u|^2\right\} = \eta\rho |h_{ru,n}|^2 \sigma_r^2 + \sigma_u^2. \tag{11}$$

Substituting (10) and (11) into $\gamma_{e2e,n}$ yields the instantaneous end-to-end SNR at the n-th port as

$$\gamma_{e2e,n} = \frac{\eta\rho P_s |h_{sr}|^2 |h_{ru,n}|^2}{\eta\rho |h_{ru,n}|^2 \sigma_r^2 + \sigma_u^2}. \tag{12}$$

Due to the correlation among $\{h_{ru,n}\}_{n=1}^{N}$ induced by $\mathbf{R}$, the set of SNRs ($\{\gamma_{e2e,n}\}_{n=1}^{N}$) is statistically dependent.

Exploiting the spatial reconfigurability of the FAS, U selects the receive port that maximizes the instantaneous channel power gain of the R–U link. Specifically, the selected port index is defined as [28]

$$n^{\star} = \arg \max_{1\leq n\leq N} |h_{ru,n}|^2. \tag{13}$$

Accordingly, the *selected* R–U channel coefficient and its corresponding power gain are given, respectively, by

$$h_{ru}^{\star} \triangleq h_{ru,n^{\star}}, \qquad |h_{ru}^{\star}|^2 = \max_{1\leq n\leq N} |h_{ru,n}|^2. \tag{14}$$

Due to the spatial correlation among the FAS ports governed by $\mathbf{R}$, the random variables ($\{|h_{ru,n}|^2\}_{n=1}^{N}$) are statistically dependent; hence, the distribution of $|h_{ru}^{\star}|^2$ differs from the conventional i.i.d. order-statistics case. Based on the port-selection rule in (13), the received signal at U is taken from the selected port output, i.e., $y_u \triangleq y_{u,n^{\star}}$. Accordingly, the received signal after selection can be expressed as

$$y_u \approx \underbrace{\sqrt{\eta\rho P_s}\, h_{sr} h_{ru}^{\star} x}_{\text{desired signal}} + \underbrace{\sqrt{\eta\rho}\, h_{ru}^{\star} w_r + w_u}_{\text{noise}}. \tag{15}$$

Therefore, under FAS-based receiver selection, the end-to-end channel is effectively characterized by the $h_{sr}h_{ru}^{\star}$ product, where $h_{ru}^{\star}$ corresponds to the maximum-gain port over the spatially correlated FAS ports. The received signal after FAS-based receiver selection is given in (15). Accordingly, the instantaneous desired-signal power equals

$$\mathbb{E}\Big\{|\text{desired signal}|^2\Big\} = \eta\rho P_s |h_{sr}|^2 |h_{ru}^{\star}|^2, \tag{16}$$

while the total noise power at U consists of the forwarded R noise and the local receiver noise, i.e.,

$$\mathbb{E}\Big\{|\text{noise}|^2\Big\} = \eta\rho |h_{ru}^{\star}|^2 \sigma_r^2 + \sigma_u^2. \tag{17}$$

Hence, the instantaneous end-to-end SNR is given by

$$\gamma_{e2e} = \frac{\eta\rho P_s |h_{sr}|^2 |h_{ru}^{\star}|^2}{\eta\rho |h_{ru}^{\star}|^2 \sigma_r^2 + \sigma_u^2}. \tag{18}$$

For convenience of presentation, we assume equal noise variances at R and U, i.e., $\sigma_r^2 = \sigma_u^2 = \sigma^2$, and define the average transmit SNR at the BS as $\bar{\gamma} \triangleq \frac{P_s}{\sigma^2}$. Substituting these into (18), the instantaneous end-to-end SNR can be rewritten as

$$\begin{aligned}\gamma_{e2e} &= \frac{\eta\rho P_s |h_{sr}|^2 |h_{ru}^{\star}|^2}{\sigma^2\left(\eta\rho |h_{ru}^{\star}|^2 + 1\right)} \\ &= \frac{\eta\rho\bar{\gamma}\, |h_{sr}|^2 |h_{ru}^{\star}|^2}{\eta\rho |h_{ru}^{\star}|^2 + 1}.\end{aligned} \tag{19}$$

3. Performance Analysis

In this section, we analytically characterize the proposed system by deriving the end-to-end SNR statistics under FAS-based receive-port selection. A copula-based framework is adopted to model the correlation among the channel gains, enabling the derivation of exact SNR distribution expressions. These results are then used to obtain the outage probability for both correlated and uncorrelated FAS-port scenarios, providing insight into the effects of power splitting, the number of ports, and spatial correlation.

3.1. End-to-End SNR Statistics

Theorem 1. *The CDF of γ_{e2e} is given by*

$$F_\gamma(g) = \int_0^\infty \left(1 - \exp\left[-\frac{g(az+1)}{a\bar{\gamma}\Omega_{sr}\, z}\right]\right) f_Z(z)\, dz, \tag{20}$$

where $f_Z(z)$ is obtained from the Gaussian copula-based selected-port CDF in (28) *via* (29).

Proof. Recall that, after FAS-based port selection, the instantaneous end-to-end SNR in (19) can be rewritten as

$$\gamma_{e2e} = \frac{a\,\bar{\gamma}\,X\,Z}{a\,Z+1}, \tag{21}$$

where

$$a \triangleq \eta\rho, \qquad X \triangleq |h_{sr}|^2, \qquad Z \triangleq |h^{\star}_{ru}|^2. \tag{22}$$

Since $h_{sr} \sim \mathcal{CN}(0, \Omega_{sr})$, the first-hop power gain ($X = |h_{sr}|^2$) is exponentially distributed with

$$F_X(x) = 1 - \exp\left(-\frac{x}{\Omega_{sr}}\right), \qquad f_X(x) = \frac{1}{\Omega_{sr}}\exp\left(-\frac{x}{\Omega_{sr}}\right). \tag{23}$$

For the second hop, each marginal $|h_{ru,n}|^2$ is also exponentially distributed with a mean of Ω_{ru}, i.e.,

$$F_0(z) = 1 - \exp\left(-\frac{z}{\Omega_{ru}}\right), \qquad f_0(z) = \frac{1}{\Omega_{ru}}\exp\left(-\frac{z}{\Omega_{ru}}\right), \tag{24}$$

while the N ports are statistically dependent due to the spatial correlation matrix ($\mathbf{R}$). We define $\mathbf{Z} = [Z_1, \ldots, Z_N]^{\mathrm{T}}$ with $Z_n = |h_{ru,n}|^2$ and $Z = \max_n Z_n$. The CDF of Z is the joint probability that all port gains are below z, i.e.,

$$F_Z(z) = \Pr\{Z \le z\} = \Pr\{Z_1 \le z, \ldots, Z_N \le z\}. \tag{25}$$

Let $u(z) \triangleq F_0(z)$. Using a copula representation for the joint distribution of $(Z_1, \ldots, Z_N)$ with identical marginals, we can write

$$F_Z(z) = C\big(u(z), \ldots, u(z)\big), \tag{26}$$

where $C(\cdot)$ is the selected copula capturing the dependence across the correlated ports.

Before applying the Gaussian copula model, we clarify the relationship between the physical spatial correlation matrix ($\mathbf{R}$) and the copula correlation matrix ($\mathbf{\Sigma}$). The matrix ($\mathbf{R}$) describes the spatial correlation among the complex channel coefficients at the FAS ports, whereas $\mathbf{\Sigma}$ characterizes the dependence structure among the corresponding channel power gains used in the Gaussian copula model. Since the outage probability and selected-port statistics are expressed in terms of channel power gains, the entries of $\mathbf{\Sigma}$ are constructed from the squared magnitudes of the normalized physical correlation coefficients as

$$[\mathbf{\Sigma}]_{i,j} = \begin{cases} 1, & i = j, \\ \left| \dfrac{[\mathbf{R}]_{i,j}}{\sqrt{[\mathbf{R}]_{i,i}[\mathbf{R}]_{j,j}}} \right|^2, & i \neq j. \end{cases} \tag{27}$$

This mapping ensures that the Gaussian copula dependence structure used in the selected-port statistics and outage analysis is directly determined by the physical spatial correlation model represented by **R**. This construction links the Gaussian copula dependence model directly to the physical port spacing and carrier wavelength through the Jakes correlation matrix (**R**).

It is worth noting that the Gaussian copula model is adopted here as an established dependence-modeling framework for correlated FAS-port gains, whose suitability and validation have been reported in prior FAS correlation studies [12]. Therefore, the focus of the present work is not to re-validate the copula model itself but, rather, to employ it to derive the outage performance of the proposed EH–AF relay-assisted FAS system under spatially correlated port fading.

In particular, under the *Gaussian copula* model, the joint CDF is [29]

$$F_Z(z) = C_G\big(u(z),\ldots,u(z);\mathbf{\Sigma}\big) = \Phi_{\mathbf{\Sigma}}\Big(\Phi^{-1}(u(z)),\ldots,\Phi^{-1}(u(z))\Big), \tag{28}$$

where $\Phi(\cdot)$ is the standard normal CDF and $\Phi_{\mathbf{\Sigma}}(\cdot)$ is the N-variate normal CDF with a correlation matrix of $\mathbf{\Sigma}$ (chosen/constructed to reflect the spatial correlation induced by **R**). The PDF of Z then follows as

$$f_Z(z) = \frac{d}{dz}F_Z(z) = \frac{d}{dz}\,C_G\big(u(z),\ldots,u(z);\mathbf{\Sigma}\big), \tag{29}$$

with $u'(z) = f_0(z)$. Conditioned on $Z = z$, (21) becomes linear in X:

$$\gamma_{e2e}\,|\,Z = z = \frac{a\bar{\gamma}z}{az+1}\,X. \tag{30}$$

Hence, using (23), the conditional CDF is

$$\begin{aligned} F_{\gamma|Z}(g\,|\,z) &= \Pr\bigg\{X \le \frac{g(az+1)}{a\bar{\gamma}z}\bigg\} \\ &= 1 - \exp\bigg(-\frac{g(az+1)}{a\bar{\gamma}\Omega_{sr}\,z}\bigg), \end{aligned} \tag{31}$$

and the conditional PDF is

$$f_{\gamma|Z}(g\,|\,z) = \frac{az+1}{a\bar{\gamma}\Omega_{sr}\,z}\exp\bigg(-\frac{g(az+1)}{a\bar{\gamma}\Omega_{sr}\,z}\bigg). \tag{32}$$

Averaging (31) over the selected-port gain (Z) yields

$$F_\gamma(g) = \mathbb{E}_Z\Big[F_{\gamma|Z}(g\,|\,Z)\Big], \tag{33}$$

which results in the end-to-end SNR CDF in (20). Similarly, results are obtained using (32), which completes the proof. □

Since the above integrals do not admit closed-form solutions in general, we focus on the special case of uncorrelated FAS ports in order to obtain tractable analytical expressions and gain further insight into the system behavior.

Corollary 1. *The CDF of γ_{e2e} in the case of uncorrelated FAS ports is given by*

$$F_\gamma(g) = 1 - 2\exp\bigg(-\frac{g}{\bar{\gamma}\Omega_{sr}}\bigg)\sum_{k=1}^{N}\binom{N}{k}(-1)^{k+1}\sqrt{\frac{k\,g}{a\bar{\gamma}\Omega_{sr}\Omega_{ru}}}\,K_1\bigg(2\sqrt{\frac{k\,g}{a\bar{\gamma}\Omega_{sr}\Omega_{ru}}}\bigg). \tag{34}$$

https://doi.org/10.3390/en19153502

Proof. Uncorrelated FAS ports imply that the R–U port channels are independent and identically distributed (i.i.d.). In particular, $\mathbf{R} = \mathbf{I}_N$ and $\{h_{ru,n}\}_{n=1}^N$ are independent with $h_{ru,n} \sim \mathcal{CN}(0, \Omega_{ru})$. According to order statistics for i.i.d. random variables, the CDF of Z, where $Z \triangleq \max_{1 \le n \le N} Z_n$ and $Z_n \triangleq |h_{ru,n}|^2$, is

$$F_Z(z) = \Pr\{Z \le z\} = \prod_{n=1}^{N} \Pr\{Z_n \le z\} = \big(F_0(z)\big)^N = \left(1 - \exp\left(-\frac{z}{\Omega_{ru}}\right)\right)^N, \tag{35}$$

and the corresponding PDF is

$$f_Z(z) = \frac{d}{dz} F_Z(z) = \frac{N}{\Omega_{ru}} \exp\left(-\frac{z}{\Omega_{ru}}\right) \left(1 - \exp\left(-\frac{z}{\Omega_{ru}}\right)\right)^{N-1}. \tag{36}$$

Binomial expansion yields the equivalent finite-sum form (Equation (1.111) in [30]):

$$F_Z(z) = \sum_{k=0}^{N} \binom{N}{k} (-1)^k \exp\left(-\frac{kz}{\Omega_{ru}}\right), \tag{37}$$

and

$$f_Z(z) = \sum_{k=1}^{N} \binom{N}{k} (-1)^{k+1} \frac{k}{\Omega_{ru}} \exp\left(-\frac{kz}{\Omega_{ru}}\right). \tag{38}$$

To obtain a tractable expression, we substitute (38) into (20) and use the identity, (Equation. (3.471.9) in [30])

$$\int_0^\infty \exp\left(-\beta z - \frac{\alpha}{z}\right) dz = 2\sqrt{\frac{\alpha}{\beta}}\, K_1\left(2\sqrt{\alpha\beta}\right),$$

where $K_\nu(\cdot)$ denotes the modified Bessel function of the second kind. First, note that

$$\exp\left[-\frac{g(az+1)}{a\bar{\gamma}\Omega_{sr}\, z}\right] = \exp\left(-\frac{g}{\bar{\gamma}\Omega_{sr}}\right) \exp\left(-\frac{g}{a\bar{\gamma}\Omega_{sr}} \frac{1}{z}\right). \tag{39}$$

Then, after algebraic manipulations, the CDF becomes

$$\begin{aligned} F_\gamma(g) &= 1 - \exp\left(-\frac{g}{\bar{\gamma}\Omega_{sr}}\right) \sum_{k=1}^{N} \binom{N}{k} (-1)^{k+1} \frac{k}{\Omega_{ru}} \int_0^\infty \exp\left(-\frac{k}{\Omega_{ru}} z - \frac{g}{a\bar{\gamma}\Omega_{sr}} \frac{1}{z}\right) dz \\ &= 1 - \exp\left(-\frac{g}{\bar{\gamma}\Omega_{sr}}\right) \sum_{k=1}^{N} \binom{N}{k} (-1)^{k+1} \frac{k}{\Omega_{ru}} \cdot 2\sqrt{\frac{\alpha}{\beta_k}}\, K_1\left(2\sqrt{\alpha\beta_k}\right), \end{aligned} \tag{40}$$

where

$$\alpha \triangleq \frac{g}{a\bar{\gamma}\Omega_{sr}}, \qquad \beta_k \triangleq \frac{k}{\Omega_{ru}}. \tag{41}$$

Equivalently, (40) can be written as in (34), which completes the proof. □

3.2. Outage Probability

Theorem 2. *The OP of the proposed system for the cases of correlated and uncorrelated FAS ports is respectively given by*

$$P_{\text{out}} = \int_0^\infty \left(1 - \exp\left[-\frac{\gamma_{\text{th}}(az+1)}{a\bar{\gamma}\Omega_{sr}\, z}\right]\right) f_Z(z)\, dz \tag{42}$$

and

$$P_{\text{out}} = 1 - 2\exp\left(-\frac{\gamma_{\text{th}}}{\bar{\gamma}\Omega_{sr}}\right)\sum_{k=1}^{N}\binom{N}{k}(-1)^{k+1}\sqrt{\frac{k\,\gamma_{\text{th}}}{a\bar{\gamma}\Omega_{sr}\Omega_{ru}}}\,K_1\left(2\sqrt{\frac{k\,\gamma_{\text{th}}}{a\bar{\gamma}\Omega_{sr}\Omega_{ru}}}\right), \tag{43}$$

where, due to half-duplex relaying, the SNR threshold corresponding to a target transmission rate (R_0) is given by $\gamma_{\text{th}} = 2^{2R_0} - 1$.

Proof. In a half-duplex R-assisted communication system, an outage event occurs when the instantaneous end-to-end SNR falls below the minimum threshold required to support a target transmission rate. Accordingly, the OP is defined as the probability that the instantaneous end-to-end SNR is less than this threshold. Mathematically, the OP is expressed as

$$P_{\text{out}} \triangleq \Pr\{\gamma_{e2e} < \gamma_{\text{th}}\}, \tag{44}$$

which directly yields $P_{\text{out}} = F_\gamma(\gamma_{\text{th}})$. By using $F_\gamma(g)$ as given in Theorem 1 and Corollary 1 for the cases of correlated and uncorrelated FAS ports, respectively, the OP expressions for both cases are obtained, which completes the proof. □

3.3. High-SNR Asymptotic Outage Probability

We next derive the high-SNR asymptotic OP for the uncorrelated FAS case. Recall that

$$P_{\text{out}} = \int_0^\infty \left(1 - \exp\left[-\frac{\gamma_{\text{th}}(az+1)}{a\bar{\gamma}\Omega_{sr}\,z}\right]\right) f_Z(z)\,dz, \qquad a \triangleq \eta\rho, \tag{45}$$

where, for i.i.d. ports,

$$f_Z(z) = \frac{N}{\Omega_{ru}}\exp\left(-\frac{z}{\Omega_{ru}}\right)\left(1 - \exp\left(-\frac{z}{\Omega_{ru}}\right)\right)^{N-1}. \tag{46}$$

Theorem 3. *For uncorrelated FAS ports with $N \geq 2$, as $\bar{\gamma} \to \infty$, the outage probability satisfies*

$$P_{\text{out}} \sim \frac{\gamma_{\text{th}}}{a\Omega_{sr}}\frac{1}{\bar{\gamma}}\left(a + \mathbb{E}\left[\frac{1}{Z}\right]\right), \qquad \bar{\gamma} \to \infty, \tag{47}$$

where $Z = \max_{1\leq n\leq N}|h_{ru,n}|^2$ and

$$\mathbb{E}\left[\frac{1}{Z}\right] = \frac{N}{\Omega_{ru}}\sum_{m=1}^{N-1}\binom{N-1}{m}(-1)^{m+1}\ln(m+1). \tag{48}$$

Proof. At high SNRs, the argument of the exponential in (45) is small. Hence, $1 - e^{-x} \approx x$ for $x \to 0$. Therefore,

$$\begin{aligned} P_{\text{out}} &\approx \int_0^\infty \frac{\gamma_{\text{th}}(az+1)}{a\bar{\gamma}\Omega_{sr}\,z} f_Z(z)\,dz \\ &= \frac{\gamma_{\text{th}}}{a\bar{\gamma}\Omega_{sr}}\mathbb{E}\left[\frac{aZ+1}{Z}\right] \\ &= \frac{\gamma_{\text{th}}}{a\bar{\gamma}\Omega_{sr}}\left(a + \mathbb{E}\left[\frac{1}{Z}\right]\right), \end{aligned} \tag{49}$$

which proves (47).

$\mathbb{E}[1/Z]$ remains to be computed. Using the i.i.d. maximum PDF and the change of variables ($t = e^{-z/\Omega_{ru}}$) so that $z = -\Omega_{ru} \ln t$ and $dz = -\Omega_{ru}\, dt/t$, we obtain

$$\begin{aligned}\mathbb{E}\left[\frac{1}{Z}\right] &= \int_0^\infty \frac{1}{z} f_Z(z)\, dz \\ &= \int_0^\infty \frac{1}{z}\, \frac{N}{\Omega_{ru}} e^{-z/\Omega_{ru}} \left(1 - e^{-z/\Omega_{ru}}\right)^{N-1} dz \\ &= \frac{N}{\Omega_{ru}} \int_0^1 \frac{(1-t)^{N-1}}{-\ln t}\, dt. \end{aligned} \tag{50}$$

Since

$$(1-t)^{N-1} = \sum_{m=0}^{N-1} \binom{N-1}{m} (-1)^m t^m, \tag{51}$$

and, for $N \geq 2$,

$$\sum_{m=0}^{N-1} \binom{N-1}{m} (-1)^m = 0, \tag{52}$$

we can rewrite

$$(1-t)^{N-1} = \sum_{m=1}^{N-1} \binom{N-1}{m} (-1)^m (t^m - 1). \tag{53}$$

Using the identity expressed as

$$\int_0^1 \frac{1-t^m}{-\ln t}\, dt = \ln(m+1), \qquad m \geq 1, \tag{54}$$

we obtain

$$\begin{aligned}\mathbb{E}\left[\frac{1}{Z}\right] &= \frac{N}{\Omega_{ru}} \sum_{m=1}^{N-1} \binom{N-1}{m} (-1)^m \int_0^1 \frac{t^m - 1}{-\ln t}\, dt \\ &= \frac{N}{\Omega_{ru}} \sum_{m=1}^{N-1} \binom{N-1}{m} (-1)^{m+1} \ln(m+1). \end{aligned} \tag{55}$$

This proves (48) and completes the proof. □

Corollary 2. *For uncorrelated FAS ports with $N \geq 2$, the system achieves a diversity order of*

$$d = 1, \tag{56}$$

and the asymptotic coding gain is

$$G_c = \left[\frac{\gamma_{\text{th}}}{a\Omega_{sr}} \left(a + \frac{N}{\Omega_{ru}} \sum_{m=1}^{N-1} \binom{N-1}{m} (-1)^{m+1} \ln(m+1) \right) \right]^{-1}. \tag{57}$$

Proof. According to (47), $P_{\text{out}} \propto \bar{\gamma}^{-1}$ as $\bar{\gamma} \to \infty$; hence, $d = 1$. The coding gain is obtained by identifying the multiplicative constant in front of $1/\bar{\gamma}$. □

4. Numerical Results

In this section, Monte Carlo simulations are conducted to validate the analytical OP expressions and to investigate the effects of the number of FAS ports, spatial correlation among FAS ports, and the power-splitting ratio on the proposed EH–AF relaying system. Unless otherwise stated, all numerical results are obtained under the following common simulation setup. A half-duplex AF relaying system is considered, where the BS–R link follows Rayleigh fading with an average channel power of $\Omega_{sr} = 1$. The R–U FAS ports also have Rayleigh fading marginals with average channel power of $\Omega_{ru} = 1$, while their spatial dependence is modeled through the correlation matrix generated by the Jakes model with normalized inter-port spacing (Δ/λ). Equal noise variances are assumed at the relay and destination, i.e., $\sigma_r^2 = \sigma_u^2 = \sigma^2$, and the average transmit SNR is defined as $\bar{\gamma} = P_s/\sigma^2$.

The relay operates with a power-splitting EH architecture, where the energy-conversion efficiency is fixed at $\eta = 0.8$ and the power-splitting ratio is denoted by ρ, yielding $a = \eta\rho$. The target transmission rate is set to $R_0 = 0.5$ bits/s/Hz, which gives the half-duplex outage threshold of $\gamma_{\mathrm{th}} = 2^{2R_0} - 1$. The average SNR range is 0–40 dB. For correlated FAS scenarios, the analytical OP in (42) is computed numerically using a Gaussian copula-based expectation approach, which avoids computationally expensive multidimensional integrations. For uncorrelated FAS ports, the OP is evaluated using the exact closed-form expression in (43). Monte Carlo simulations are performed using 2×10^5 independent channel realizations in MATLAB R2017a, while 3×10^5 samples are used for the Gaussian copula-based numerical expectation. The investigated FAS-port numbers, normalized port spacings, and power-splitting ratios are specified in the corresponding figure captions.

As a baseline, a conventional fixed-antenna receiver is considered throughout the numerical results. In this benchmark, the destination user is equipped with a single antenna port and does not employ spatial adaptation or FAS-based port selection.

For clarity, a consistent plotting convention is used throughout the numerical results. Analytical results are shown by continuous curves, whereas Monte Carlo simulation results are shown by discrete markers. The correlated, uncorrelated, and parameter-dependent cases are kept in the same plots to allow for direct visual comparison under identical axes and simulation settings. This presentation avoids repeating similar sub-figures while preserving the theory–simulation comparison for each investigated scenario.

4.1. Impact of the Number of FAS Ports

Figure 2 illustrates the OP versus SNR for the proposed system under spatially correlated and uncorrelated ports for different numbers of candidate ports (N). In this comparison, the normalized inter-port spacing is kept fixed at $\Delta/\lambda = 0.2$ as N increases from 4 to 16; therefore, the total FAS aperture increases with N. In this figure, Monte Carlo simulation results are plotted together with the corresponding theoretical curves obtained from the Gaussian copula-based integral expression in (42) for spatially correlated ports. In contrast, they are obtained from (43) for spatially uncorrelated ports. First, the theoretical results closely match the simulation curves over the entire SNR range for all N values. This confirms the accuracy of the derived end-to-end SNR in (19) and the Gaussian copula model used to characterize the distribution of the selected FAS port gain under spatial correlation. Minor deviations can occur due to numerical integration errors and finite Monte Carlo averaging. From a performance perspective, the OP decreases monotonically with an increasing SNR, as expected. More importantly, increasing the number of FAS ports significantly enhances the outage performance, even in the presence of spatial correlation. This can be due to the selection criterion provided by the FAS, whereas U dynamically activates the port corresponding to the maximum instantaneous R–U channel power gain. Moreover, in all cases, the FAS-based receiver clearly outperforms the fixed-antenna baseline, which confirms the effectiveness and robustness of the proposed architecture. For example, to achieve an OP of 10^{-2}, the FAS provides approximately 7.5 dB and 10 dB SNR gains over the fixed-antenna scheme when $N = 4$ and $N = 16$ ports are employed, respectively.

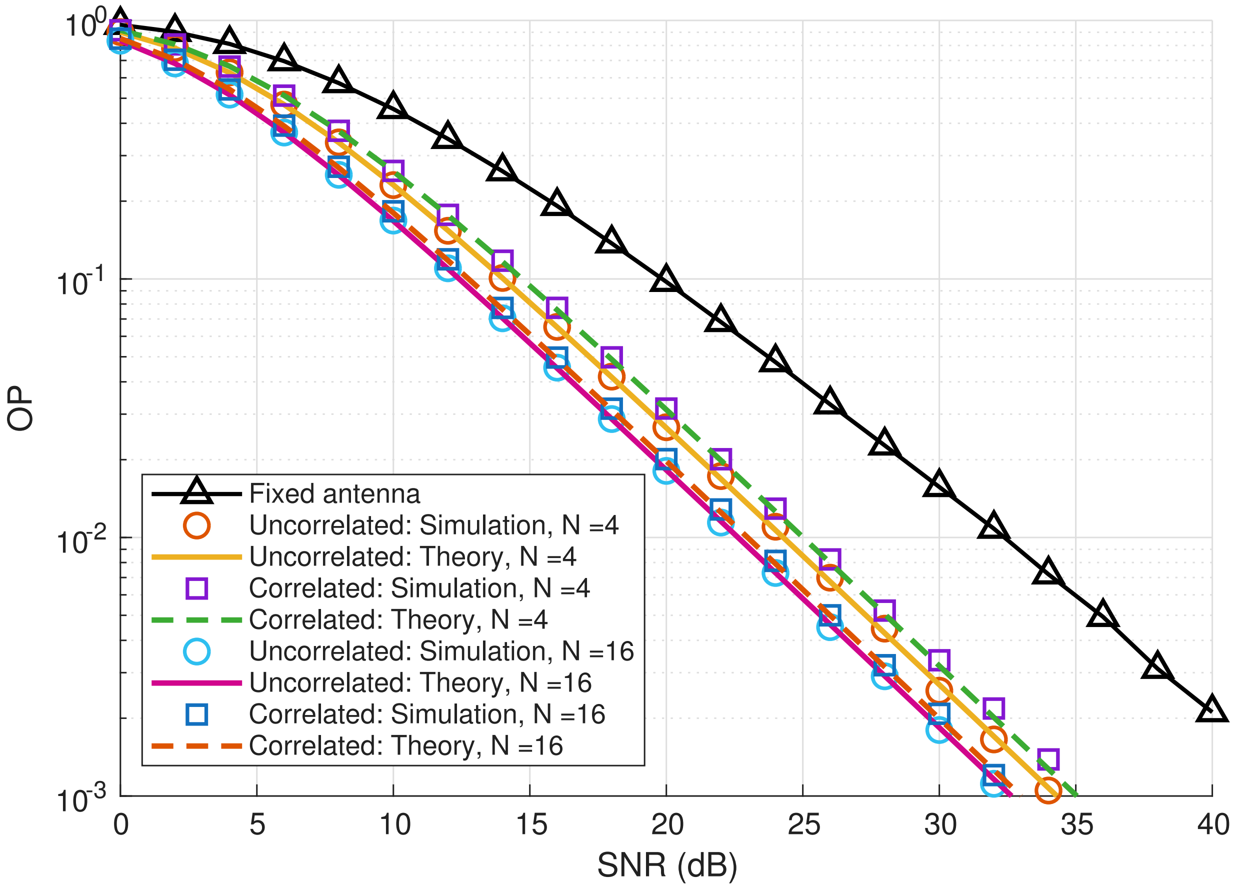

Figure 2. OP versus average-transmit SNR for different numbers of FAS ports ($N \in \{4, 16\}$) under correlated ($\Delta/\lambda = 0.2$) and uncorrelated port conditions.

4.2. Effect of Spatial Correlation

Figure 3 illustrates the impact of spatial correlation on the OP performance of the proposed system. The OP is plotted as a function of the average transmit SNR for different normalized inter-port spacings (Δ/λ), with the number of candidate ports fixed at $N = 8$. From a performance perspective, spatial correlation has an apparently detrimental effect on outage behavior. As the inter-port spacing (Δ/λ) decreases, the correlation among the FAS ports becomes stronger, leading to a noticeable degradation in OP performance. This degradation is caused by reduced statistical independence among the port-channel gains, which limits the achievable selection diversity. In contrast, as Δ/λ increases, the spatial correlation weakens, and the outage curves gradually approach the uncorrelated benchmark, indicating that the diversity loss vanishes when the ports are sufficiently separated. These results highlight the critical role of spatial correlation in practical FAS deployments and demonstrate that, although FAS-based receiver selection remains beneficial under correlated conditions, its performance is strongly influenced by the physical spacing between antenna ports. Consequently, appropriate FAS geometry design is essential to fully exploit the potential diversity gains offered by fluid-antenna systems.

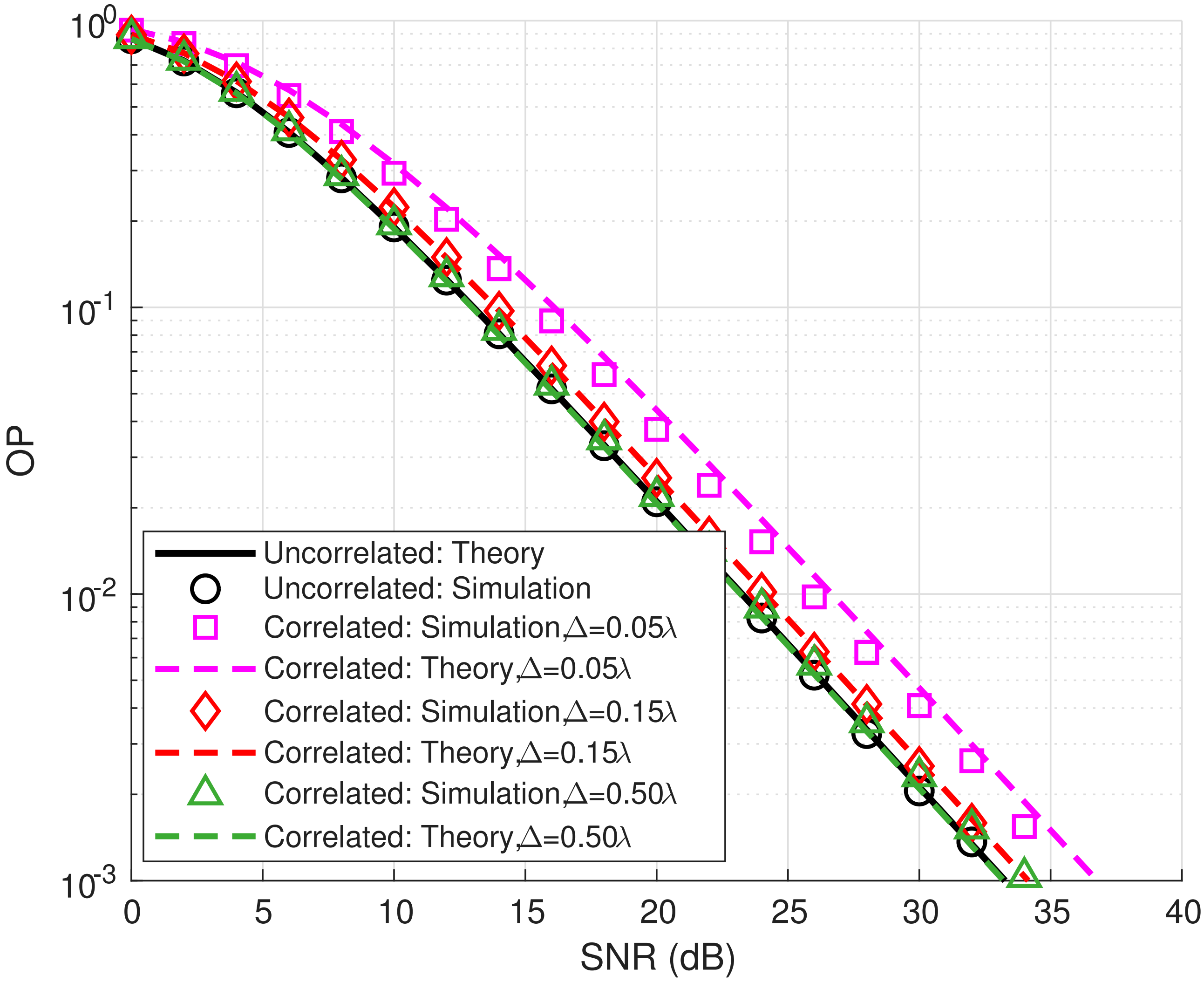

Figure 3. OP versus average-transmit SNR for different correlation strengths (Δ/λ) with a fixed $N = 8$.

4.3. Influence of the Power-Splitting Ratio

Figure 4 examines how the power-splitting ratio (ρ) affects the OP of the proposed EH-enabled AF relaying system with FAS-based receiver selection. In this evaluation, the destination is equipped with $N = 8$ spatially correlated FAS ports, with an inter-port spacing of $\Delta = 0.2\lambda$. A clear dependence on ρ can be observed. When a larger fraction of the received power is assigned to energy harvesting, the relay becomes capable of transmitting with higher forwarding power through the factor expresses as $a = \eta\rho$. This directly improves the strength of the relayed signal. Consequently, the OP decreases as ρ increases over the considered SNR range. The case of $\rho = 0.9$ achieves the best reliability among the tested configurations, whereas $\rho = 0.1$ exhibits the weakest outage performance because the harvested energy is insufficient to support effective relay transmission. This trend is particularly important in the considered system, since the direct BS–U link is assumed to be unavailable. Under such a condition, the relay is the only communication path, and any limitation in harvested energy immediately affects the end-to-end link reliability. Nevertheless, the improvement obtained by increasing ρ should not be interpreted as an unlimited design rule. In practical power-splitting receivers, assigning too much received power to the EH branch may reduce the signal power available for information processing, which can weaken the quality of the signal handled by the relay. Therefore, the selection of ρ should generally reflect a trade-off between harvested energy and information-processing capability. For the system parameters considered in Figure 4, however, the numerical results indicate that using a relatively large power-splitting ratio is beneficial for reducing the OP, even when the FAS ports are strongly correlated. This figure shows the validation of the high-SNR approximated relay-gain model against the exact variable-gain AF model for different power-splitting ratios (ρ). The comparison is shown over the low- and medium-SNR regions to examine the accuracy of the approximation used in the analytical outage analysis. The exact end-to-end SNR at the nth FAS port used to generate the exact-gain curves in Figure 4 is expressed as

$$\gamma_{\mathrm{e2e},n}^{\mathrm{exact}} = \frac{G^2(1-\rho)P_s|h_{sr}|^2|h_{ru,n}|^2}{G^2(1-\rho)|h_{ru,n}|^2\sigma_r^2 + \sigma_u^2}, \tag{58}$$

where G is the exact relay gain given in (6). For each Monte Carlo realization, G is computed from the instantaneous BS–R channel, and $\gamma_{\mathrm{e2e},n}^{\mathrm{exact}}$ is evaluated for all N FAS ports. The selected-port SNR is then obtained as $\gamma_{\mathrm{e2e}}^{\mathrm{exact}} = \max_{1\le n\le N} \gamma_{\mathrm{e2e},n}^{\mathrm{exact}}$. An outage is recorded when $\gamma_{\mathrm{e2e}}^{\mathrm{exact}} < \gamma_{\mathrm{th}}$, and the exact-gain OP is estimated over the same 2×10^5 independent channel realizations used for the other Monte Carlo results.

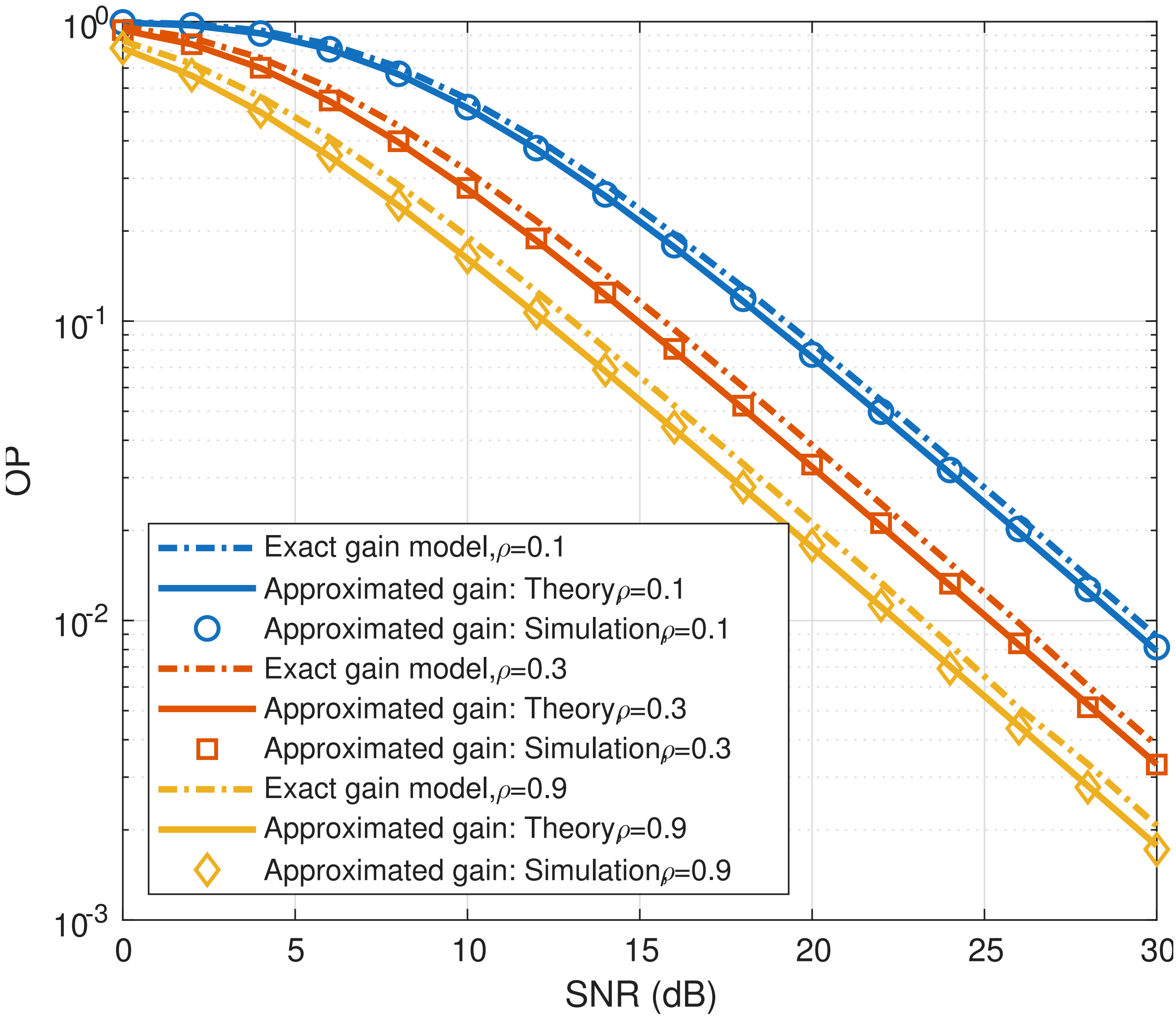

Figure 4. OP versus average-transmit SNR for different power-splitting ratios ($\rho \in \{0.1, 0.3, 0.9\}$) with fixed $N = 8$ and $\Delta = 0.2\lambda$.

4.4. Impact of the Power-Splitting Ratio over the Tested Range

Figure 5 presents the OP as a function of the power-splitting ratio (ρ) for both uncorrelated and spatially correlated FAS-port configurations under different average-transmit SNR values. In addition, Figure 5 highlights the best-performing power-splitting ratio within the tested range, denoted by ρ_{best}, which corresponds to the evaluated value of ρ that yields the lowest observed OP for each considered system setting. A pronounced dependence on ρ is evident. As the power-splitting ratio increases, a larger fraction of the received signal power at the relay is directed toward energy harvesting, thereby increasing the available forwarding power through the factor expressed as $a = \eta\rho$. This additional harvested energy improves the strength of the relayed signal and reduces the probability of outage. For the considered parameter range, the OP exhibits a monotonically decreasing trend with respect to ρ in both the uncorrelated and correlated FAS cases. Accordingly, $\rho_{best} = 0.9$, the upper endpoint of the tested range, yields the lowest observed OP among the evaluated values of ρ; therefore, no genuine interior optimum is established.

This observation is based on the adopted high-SNR approximated relay-gain model and the considered simulation setup. Therefore, the improvement in OP with increasing ρ should be interpreted as a model-dependent observation rather than a general design rule for all EH–AF relay systems. When the exact relay-gain model is retained, the effect of ρ may depend on the interaction among harvested energy, relay amplification, and forwarded relay noise.

It should be noted that the conclusions related to large power-splitting ratios are interpreted under the adopted high-SNR approximated relay-gain model. Although this approximation is commonly used in EH–AF relaying analysis, extremely large values of ρ may require additional investigation using the exact relay-gain expression, since the balance between harvested relay power, information-processing power, and forwarded relay noise can affect the observed outage behavior. Under the adopted high-SNR approximated relay-gain model, the OP decreases monotonically with ρ over the tested range. Therefore, Figure 5 should not be interpreted as identifying a genuine interior optimum. Rather, it shows that $\rho = 0.9$ provides the lowest OP among the tested values of ρ for the considered system parameters. This observation is model- and parameter-dependent and should not be regarded as a universally applicable power-splitting design rule.

This observation indicates that relay energy availability is a dominant factor in the outage behavior of the proposed EH-assisted AF relaying system. The influence of spatial correlation is also clear. Compared with the uncorrelated case, correlated FAS ports produce higher OP values over the entire range of ρ, mainly because spatial dependence reduces the effective selection diversity among the receive ports. The degradation is noticeable, but the general shape of the outage curves remains unchanged. For both the correlated and uncorrelated cases, $\rho_{best} = 0.9$ remains the best-performing value within the tested range. This indicates that spatial correlation affects the achievable outage level but does not change the observed monotonic dependence on ρ within the investigated range. Increasing the average-transmit SNR shifts all outage curves downward, as expected, since a stronger transmit signal improves the end-to-end link quality. However, the overall behavior with respect to ρ remains consistent across the examined SNR regimes. These findings provide an important design implication: in the considered EH-enabled AF relaying system with FAS-based receiver selection, assigning a relatively large portion of the received power to energy harvesting can be beneficial in terms of minimizing OP, even when the FAS ports are spatially correlated.

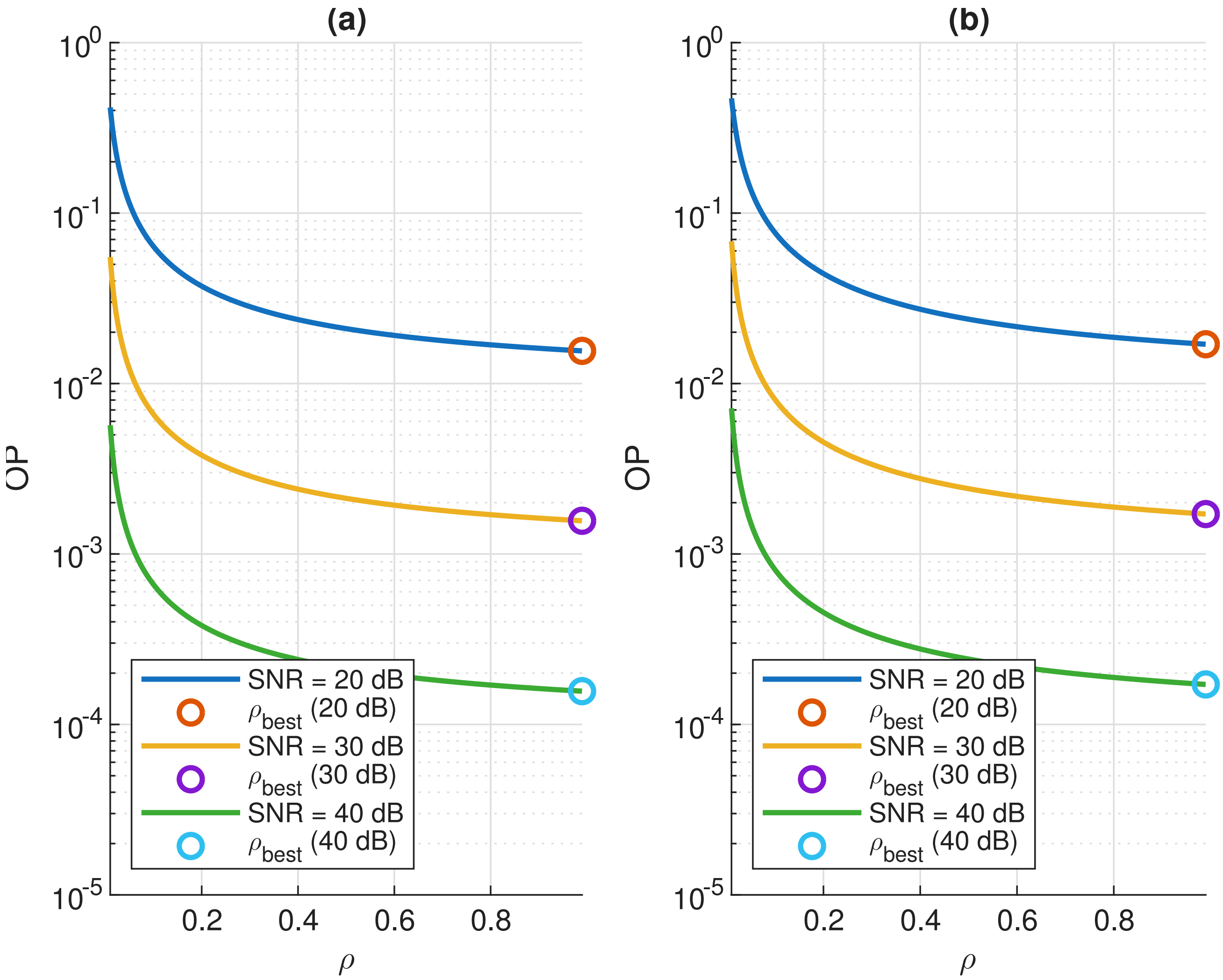

Figure 5. OP versus power-splitting ratio (ρ) for different average-transmit SNR values: (**a**) uncorrelated FAS ports; (**b**) correlated FAS ports with fixed $N = 8$ and $\Delta = 0.2\lambda$.

4.5. Validation of the Selected-Port Statistics

Figures 6–8 provide a visual validation of the Gaussian copula-based selected-port distribution for different numbers of FAS ports ($N = \{4, 8, 16\}$) and normalized port spacings ($\Delta/\lambda = \{0.05, 0.2, 0.5\}$). In each case, the left subfigure compares the empirical CDF of the selected-port gain ($Z = \max_{1 \leq n \leq N} |h_{ru,n}|^2$) obtained from correlated Rayleigh fading simulations with the Gaussian copula-based CDF constructed using $\Sigma_{ij} = |R_{ij}|^2$. The right subfigure compares the corresponding empirical and copula-based PDFs. Close agreement between the empirical curves and the Gaussian copula curves is observed for all tested values of N and Δ/λ. This agreement indicates that the adopted Gaussian copula model accurately captures the distribution of the maximum selected FAS-port gain. As N increases, the selected-port gain shifts toward larger values because the receiver has more candidate ports and can select a stronger channel realization. This behavior is also reproduced by the copula-based model. The figure further illustrates the effect of the normalized port spacing (Δ/λ). For small spacing, such as $\Delta/\lambda = 0.05$, the FAS ports are strongly correlated, which reduces the selection diversity and limits the shift of the selected-port distribution toward higher gain values. As Δ/λ increases, the spatial correlation becomes weaker, and the selected-port gain improves because the ports provide more independent fading observations. The Gaussian copula model follows this trend well for all considered spacings. The visual validation in Figures 6–8 is further supported by the quantitative results in Table 2. The KS distance and CDF-RMSE are computed between the empirical selected-port CDF and the Gaussian copula-based selected-port CDF. In addition, the mean power-correlation error measures the average absolute difference between the empirical correlation of the simulated channel power gains and the adopted copula correlation matrix ($\Sigma_{ij} = |R_{ij}|^2$). Across all tested configurations, the KS distance remains below 5.7043×10^{-2}, the CDF-RMSE remains below 2.6138×10^{-2}, and the mean power-correlation error remains below 1.8790×10^{-3}. These results provide quantitative support for the use of the Gaussian copula model in the correlated-port outage analysis.

Table 2. Quantitative validation of the Gaussian-copula selected-port distribution for different numbers of FAS ports and normalized port spacings.

N	Δ/λ	KS Distance	CDF-RMSE	Mean Power-Correlation Error
4	0.05	2.3423×10^{-2}	7.3412×10^{-3}	8.7181×10^{-4}
8	0.05	2.4977×10^{-2}	1.3267×10^{-2}	3.9392×10^{-4}
16	0.05	4.7707×10^{-2}	2.4913×10^{-2}	1.2847×10^{-3}
4	0.20	2.7413×10^{-2}	1.3251×10^{-2}	1.1819×10^{-3}
8	0.20	4.3710×10^{-2}	2.1058×10^{-2}	1.8790×10^{-3}
16	0.20	5.7043×10^{-2}	2.6138×10^{-2}	1.4669×10^{-3}
4	0.50	5.9900×10^{-3}	2.6902×10^{-3}	1.6213×10^{-3}
8	0.50	1.1143×10^{-2}	4.4967×10^{-3}	1.8641×10^{-3}
16	0.50	1.5317×10^{-2}	6.2058×10^{-3}	1.5310×10^{-3}

In the numerical results, the energy conversion efficiency (η), target rate, and average channel powers are fixed in order to isolate the effects of the FAS-port number, spatial correlation, and power-splitting factor on the outage probability. Therefore, the reported performance trends should be interpreted under the considered parameter settings.

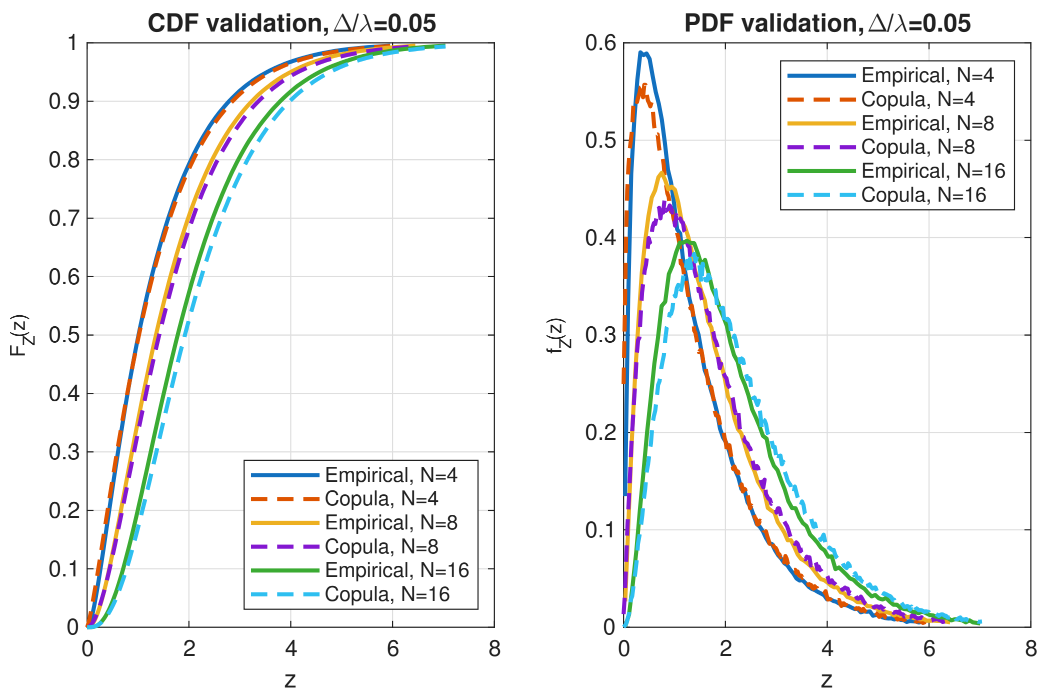

Figure 6. Validation of selected-port statistics under correlated FAS ports: (**left**) empirical and Gaussian copula-based CDFs ($F_Z(z)$); (**right**) corresponding PDFs ($f_Z(z)$) of $Z = \max_{1 \le n \le N} |h_{ru,n}|^2$ for different values of N and $\Delta = 0.05\lambda$.

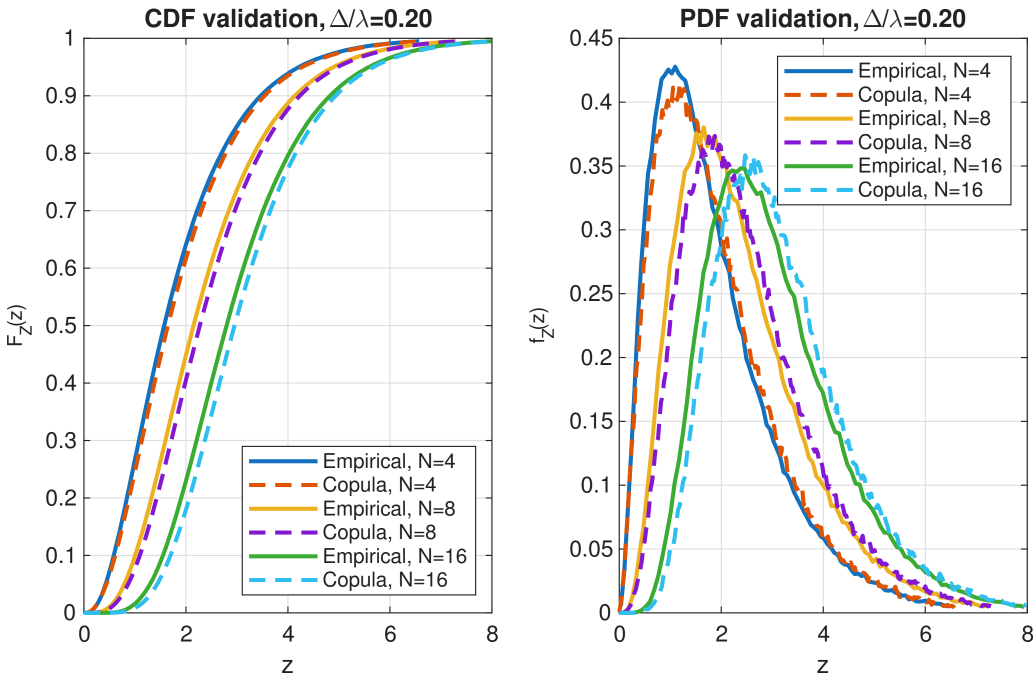

Figure 7. Validation of selected-port statistics under correlated FAS ports: (**left**) empirical and Gaussian copula-based CDFs ($F_Z(z)$); (**right**) corresponding PDFs ($f_Z(z)$) of $Z = \max_{1\leq n\leq N} |h_{ru,n}|^2$ for different values of N and $\Delta = 0.2\lambda$.

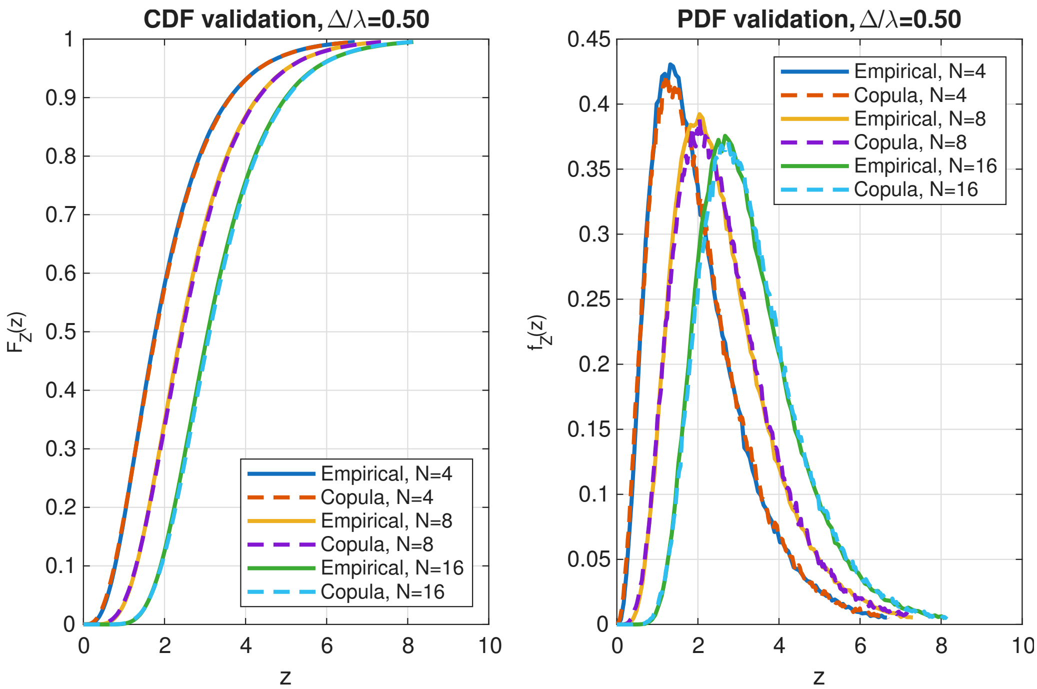

Figure 8. Validation of selected-port statistics under correlated FAS ports: (**left**) empirical and Gaussian copula-based CDFs ($F_Z(z)$); (**right**) corresponding PDFs ($f_Z(z)$) of $Z = \max_{1\leq n\leq N} |h_{ru,n}|^2$ for different values of N and $\Delta = 0.5\lambda$.

5. Conclusions

This paper presented a comprehensive performance analysis of an FAS-assisted EH–AF R network, where the direct link between the BS and U is unavailable. By incorporating FAS-based receive-port selection at U and PS-based EH at R, the proposed system effectively exploits spatial diversity and harvested energy to enhance communication reliability. To accurately model the spatial correlation inherent to closely spaced fluid-antenna ports, a Gaussian copula framework was adopted, enabling a tractable characterization of the channel statistics for the selected port. Exact integral expressions for the end-to-end SNR distribution and OP were derived for the general correlated case, while closed-form expressions were obtained for uncorrelated FAS ports. Monte Carlo simulations verified the accuracy of the analytical results. They confirmed the validity of the copula-based modeling approach through close agreement between empirical and analytical CDFs and PDFs of the selected-port gain. The numerical results demonstrated that increasing the number of FAS ports yields significant improvements in outage performance, whereas spatial correlation reduces achievable selection diversity and degrades reliability. Furthermore, under the adopted high-SNR approximated relay-gain model, the PS ratio has a pronounced influence on the outage performance. Across the investigated range, the OP decreases monotonically as ρ increases, with $\rho = 0.9$, the considered upper endpoint, yielding the lowest observed OP. This behavior is specific to the adopted approximation and the examined system parameters and, therefore, should not be interpreted as establishing a universally applicable operating point or as general design guidance for practical EH–AF relay systems. Future research can extend the proposed analytical framework to more generalized fading models, multi-relay and multi-user network configurations, imperfect channel-state information, and adaptive power-splitting mechanisms capable of dynamically balancing information decoding and energy harvesting according to instantaneous channel conditions.

Author Contributions: Conceptualization, K.Y. and M.A.; Methodology, K.Y. and M.A.; Software, K.Y. and M.A.; Validation, K.Y., M.A. and S.A.K.; Formal analysis, K.Y. and S.A.K.; Investigation, K.Y. and B.A.A.; Resources, M.A.; Data curation, K.Y. and S.A.K.; Writing—original draft, K.Y. and M.A.; Writing—review & editing, M.A., B.A.A., S.A.D. and S.A.K.; Visualization, M.A.; Supervision, K.Y.; Project administration, K.Y.; Funding acquisition, S.A.D. All authors have read and agreed to the published version of the manuscript.

Funding: This research received no external funding.

Data Availability Statement: The original contributions presented in the study are included in the article, further inquiries can be directed to the corresponding author.

Conflicts of Interest: The authors declare no conflict of interest.

References

1. Dang, S.; Amin, O.; Shihada, B.; Alouini, M.-S. What should 6G be? *Nat. Electron.* **2020**, *3*, 20–29. [CrossRef]
2. Banafaa, M.; Shayea, I.; Din, J.; Azmi, M.H.; Alashbi, A.; Daradkeh, Y.I.; Alhammadi, A. 6G Mobile Communication Technology: Requirements, Targets, Applications, Challenges, Advantages, and Opportunities. *Alex. Eng. J.* **2023**, *64*, 245–274. [CrossRef]
3. Sharma, S.; Popli, R.; Singh, S.; Chhabra, G.; Saini, G.S.; Singh, M.; Sandhu, A.; Sharma, A.; Kumar, R. The Role of 6G Technologies in Advancing Smart City Applications: Opportunities and Challenges. *Sustainability* **2024**, *16*, 7039. [CrossRef]
4. Das, M.; Nag, A.; Hassan, M.M.; Santra, A.; Chand, N.; Yasmin, F.; Sinha, A.; Bairagi, A.K.; Alkhayyat, A. Synergy of 6G Technology and IoT Networks for Transformative Applications. *Int. J. Commun. Syst.* **2024**, *37*, e5869. [CrossRef]
5. Zhang, Y.; Luo, Z.; Wu, W.; Tian, W. RIS-UAV Cooperative ISAC Technology for 6G: Architecture, Optimization, and Challenges. *Algorithms* **2026**, *19*, 65. [CrossRef]
6. Luan, N.; Xiong, K.; Zhang, Z.; Zheng, H.; Zhang, Y.; Fan, P.; Qu, G. Age-Aware Utility Maximization in Relay-Assisted Wireless Powered Communication Networks. *Entropy* **2021**, *23*, 1177. [CrossRef] [PubMed]
7. Babu, C.H.R.; Nandakumar, S. Towards Energy-Efficient Joint Relay Selection and Resource Allocation for D2D Communication Using Hybrid Heuristic-Based Deep Learning. *Sci. Rep.* **2025**, *15*, 25179. [CrossRef] [PubMed]
8. Wang, X.; Yu, D.; Liu, Y. Capacity Enhancement in Multirelay-Assisted Hybrid SWIPT Wireless Communications. *J. Inf. Intell.* **2025**, *3*, 504–514. [CrossRef]
9. Alqahtani, A.; Taneja, N.; Taneja, A.; Alqahtani, N. Energy Aware Resource Management in 6G IoT Networks Using STAR RIS. *Sci. Rep.* **2025**, *15*, 20941. [CrossRef] [PubMed]

10. New, W.K.; Wong, K.-K.; Xu, H.; Wang, C.; Rostami Ghadi, F.; Zhang, J.; Rao, J.; Murch, R.; Ramírez-Espinosa, P.; Morales-Jimenez, D.; et al. A Tutorial on Fluid Antenna System for 6G Networks: Encompassing Communication Theory, Optimization Methods and Hardware Designs. *arXiv* **2024**, arXiv:2407.03449.
11. Shah, A.F.M.S.; Karabulut, M.A.; Cinar, E.; Rabie, K.M. A Survey on Fluid Antenna Multiple Access for 6G: A New Multiple Access Technology That Provides Great Diversity in a Small Space. *IEEE Access* **2024**, *12*, 88410–88425. [CrossRef]
12. Ramírez-Espinosa, P.; Morales-Jimenez, D.; Wong, K.-K. A New Spatial Block-Correlation Model for Fluid Antenna Systems. *IEEE Trans. Wirel. Commun.* **2024**, *23*, 15829–15843. [CrossRef]
13. Xu, R.; Chen, Y.; Kang, J.; Xu, M.; Yang, Z.; Huang, C.; Niyato, D. Fluid Antenna Relay Assisted Communication Systems Through Antenna Location Optimization. In Proceedings of the 2024 IEEE International Conference on Communications Workshops (ICC Workshops), Denver, CO, USA, 9–13 June 2024; pp. 1140–1145. [CrossRef]
14. Aka, B.E.; New, W.K.; Leow, C.Y.; Wong, K.-K.; Shin, H. Power Minimization for Half-Duplex Relay in Fluid Antenna System. *IEEE Wirel. Commun. Lett.* **2025**, *14*, 1698–1702. [CrossRef]
15. Xu, R.; Yang, Z.; Zhang, Z.; Shikh-Bahaei, M.; Huang, K.; Niyato, D. Energy Efficient Fluid Antenna Relay (FAR)-Assisted Wireless Communications. *arXiv* **2025**, arXiv:2508.04322. [CrossRef]
16. Xu, R.; Yang, Z.; Zhang, T.; Chen, M.; Zhu, C.; Zhang, Z. Fair Rate Maximization for Fluid Antenna Relay (FAR)-Assisted Multi-User MISO Communications. *arXiv* **2025**, arXiv:2507.00529. [CrossRef]
17. Xu, R.; Chen, M.; Yang, Z.; Zhang, Z.; Wong, K.-K.; Chae, C.B.; Poor, H.V. Energy Efficient Fluid Antenna Relay (FAR)-Assisted Wireless Networks. In Proceedings of the GLOBECOM 2025–2025 IEEE Global Communications Conference, Taipei, Taiwan, 8–12 December 2025; pp. 6418–6423. [CrossRef]
18. Xu, R.; Zhang, S.; Yang, Z.; Chen, M.; Zhang, Z.; Wong, K.-K. Fluid Antenna Relay (FAR)-Assisted Communication with Hybrid Relaying Scheme Selection. *arXiv* **2026**, arXiv:2601.12924. [CrossRef]
19. Xu, R.; Zhang, S.; Yang, Z.; Chen, Y.; Chen, M.; Zhang, Z.; Wong, K.-K. On Performance of Fluid Antenna Relay (FAR)-Assisted AAV-NOMA Wireless Network. *arXiv* **2026**, arXiv:2603.24954. [CrossRef]
20. Xin, J.; Liang, G.; Li, L.; Ni, X.; Xia, L.; Feng, Y. Energy Efficiency Resource Allocation for Amplify and Forward Relaying System with Energy Harvesting. *Wirel. Power Transf.* **2026**, *13*, e004. [CrossRef]
21. Singh, K.R.; Garg, P. Two Way Amplify and Forward Relay with Energy Harvesting: Performance Analysis. *Comput. Electr. Eng.* **2025**, *128*, 110762. [CrossRef]
22. Kapucu, N.; Bilim, M. ASER Analysis of Fluid Antenna Systems with Rectangular and Hexagonal QAM Schemes. *AEU Int. J. Electron. Commun.* **2025**, *196*, 155792. [CrossRef]
23. Zhang, Z.; Wong, K.-K.; Morales-Jimenez, D.; Jiang, H.; Ramírez-Espinosa, P.; Chae, C.-B.; Masouros, C. Finite-Blocklength Fluid Antenna Systems with Spatial Block-Correlation Channel Model. *arXiv* **2025**, arXiv:2509.24333.
24. Stüber, G.L. *Principles of Mobile Communication*; Springer: Boston, MA, USA, 2011.
25. Krikidis, I.; Timotheou, S.; Nikolaou, S.; Zheng, G.; Ng, D.W.K.; Schober, R. Simultaneous Wireless Information and Power Transfer in Modern Communication Systems. *IEEE Commun. Mag.* **2014**, *52*, 104–110. [CrossRef]
26. Hasna, M.O.; Alouini, M.-S. End-to-End Performance of Transmission Systems with Relays over Rayleigh-Fading Channels. *IEEE Trans. Wirel. Commun.* **2003**, *2*, 1126–1131. [CrossRef]
27. Aldababsa, M. Performance of TAS/MRC in NOMA Energy Harvesting Relay Networks. *AEU Int. J. Electron. Commun.* **2023**, *162*, 154569. [CrossRef]
28. Chai, Z.; Wong, K.-K.; Tong, K.-F.; Chen, Y.; Zhang, Y. Port Selection for Fluid Antenna Systems. *IEEE Commun. Lett.* **2022**, *26*, 1180–1184. [CrossRef]
29. Aldababsa, M.; Elganimi, T.Y.; Albreem, M.A.; Abdallah, S. Novel Selection Schemes for Multi-RIS-Assisted Fluid Antenna Systems. *Phys. Commun.* **2026**, *74*, 102947. [CrossRef]
30. Gradshteyn, I.S.; Ryzhik, I.M.; Jeffrey, A.; Zwillinger, D. *Table of Integrals, Series, and Products*; Academic Press: Amsterdam, The Netherlands, 2007.

https://doi.org/10.3390/en19153502